JOURNAL OF QUATERNARY SCIENCE (1998) **13** (6) 539–547
CCC 0267-8179/98/060539–09$17.50

Relic permafrost structures in the Gobi of Mongolia: age and significance

LEWIS A. OWEN[1]*, BEN RICHARDS[2], EDWARD J. RHODES[2], W. DICKSON CUNNINGHAM[3], BRIAN F. WINDLEY[3], J. BADAMGARAV[4] and D. DORJNAMJAA[4]
[1]Department of Earth Sciences, University of California, Riverside, CA 92521-0423, USA
[2]Department of Geography, Royal Holloway, University of London, Egham, Surrey TW20 0EX, England
[3]Department of Geology, University of Leicester, Leicester LE1 7RH, England
[4]Geological Institute, Mongolian Academy of Sciences, Peace Avenue, Ulaanbaatar 20351, Mongolia

Lewis A. Owen, Ben Richards, Edward J. Rhodes, W. Dickson Cunningham, Brian F Windley, J. Badamgarav and D. Dorjnamjaa 1998. Relic permafrost structures in the Gobi of Mongolia: age and significance *J. Quaternary Sci.*, **Vol. 13**, pp. 539–547. ISSN 0267-8179
Received 4 April 1998; Revised 5 May 1998; Accepted 7 May 1998

ABSTRACT: Relict permafrost structures (ice-wedge casts and cryoturbation structures) are present in the Gobi of southern Mongolia. Luminescence dates of sediments are presented to constrain the age of formation of permafrost structures. These data show that there was a phase of permafrost development during the latter part of the Last Glacial (after about 22 to 15 ka) that resulted in cryoturbated sediments and ice-wedge casts. Furthermore, permafrost degradation occurred during late Pleistocene times (13–10 ka) and was absent during the early Holocene. These permafrost structures mark the southernmost evidence of permafrost in northern Asia during late Quaternary times and indicate that the mean annual air temperature was below approximately –6°C during their formation. © 1998 John Wiley & Sons, Ltd.

KEYWORDS: Mongolia; cryostratigraphy; ice-wedge casts; cryoturbation; luminescence dating.

Introduction

The Gobi of Mongolia comprises an extensive desert that is dominantly of reg type, consisting of alluvial fans and deeply eroded badlands with elevations between 1000 and 2000 m a.s.l. A series of narrow east–west trending mountain ranges, the Gobi Altai Mountains, cross the Gobi and reaches a maximum elevation of ca. 3900 m a.s.l. (Fig. 1). The climate is of semi-arid continental type, with summer temperatures that exceed 40°C and winter temperatures that frequently drop below –40°C. In the winter, the region is influenced by the Mongolian High Pressure System, which drives strong westerly winds and produces snow. Most streams are ephemeral, filling during heavy rainstorms and/or at higher elevations as snow melts in the spring time. Today, permafrost is absent throughout the deserts, but is present as isolated patches at high elevations in the Gobi Altai Mountains. Throughout the desert regions, however, there is much sedimentological and geomorphological evidence for the former existence of extensive permafrost (e.g. Gravis, 1974; Devyatkin, 1981). Owen *et al.* (1997) tentatively suggested that permafrost developed in alluvial fans during the Last Glacial and degraded with climatic amelioration during early Holocene times. This paper will describe the characteristics of the active layer and permafrost structures in the Gobi and will present luminescence dates to constrain the timing of permafrost development and its degradation.

* Correspondence to: Lewis A. Owen, Department of Earth Sciences, University of California, Riverside, CA 92521-0423, USA.

Contract grant sponsor: Natural Environment Research Council (UK)
Contract grant number: GR9/1517

Field methods

Field work was undertaken throughout the Gobi and the locations of permafrost structures were recorded using a global positioning system (Fig. 1). The style of permafrost structures was noted (see Figs 2–9) and samples for optically stimulated luminescence (OSL) and infra-red stimulated luminescence (IRSL) dating were collected from key locations. Samples for luminescence dating were also collected from stratigraphically younger fanglomerates and alluvium that did not exhibit any permafrost structures.

OSL dating methods and results

Sample collection and preparation

The location and stratigraphic setting of each sample for luminescence dating is described in the next section of this paper. Each of the sediment samples was collected in an opaque plastic tube and placed into a light tight bag, which

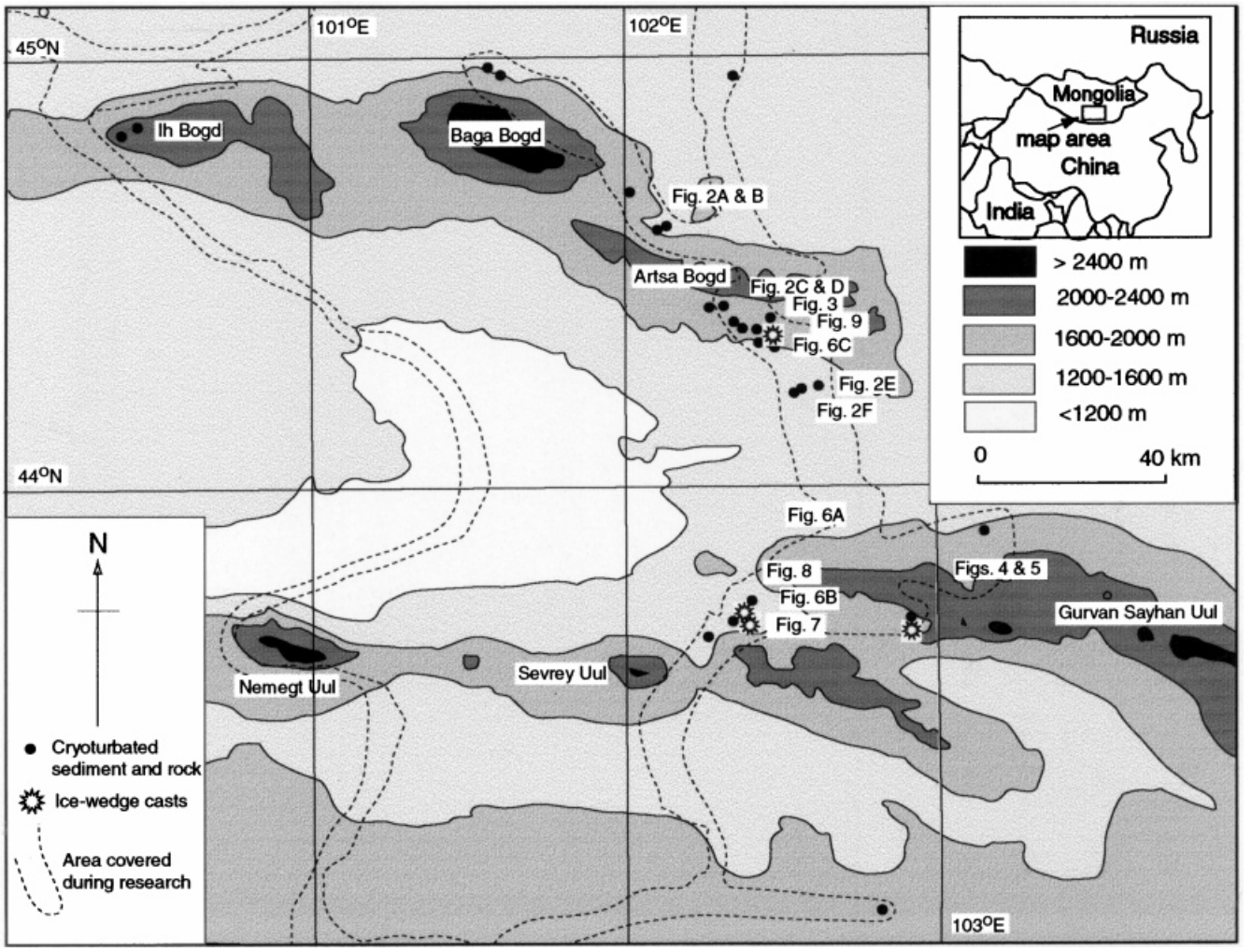

Figure 1 Map of the Gobi of Mongolia showing the locations of permafrost structures and the areas examined during this research. The locations of Figures 2 to 9 are shown.

remained sealed until opened under controlled laboratory lighting. Each sample was dried at 50°C and dependent on the particle size distribution of the samples, the 90–125 μm and/or 4–11 μm fractions were separated by dry sieving. The 90–125 μm fraction was treated with dilute hydrochloric acid to remove any carbonates, and 10% hydrogen peroxide was used to remove organic matter. Minerals less dense than 2.62 g cm^{-3} (mainly feldspars) were removed using a sodium polytungstate solution. The remaining material was subsequently treated with 40% hydrofluoric acid (HF) both to dissolve remaining feldspar grains and to etch off the outer alpha-irradiated layers of the quartz, and then washed in 10% hydrochloric acid and oven dried at 50°C. The quartz fraction was separated from heavy minerals using a sodium polytungstate solution of density 2.68 g cm^{-3}. The quartz fraction of each sample was then treated with concentrated fluorosilicic acid (H_2SiF_6) for 5–7 days to dissolve any remaining feldspar grains. The resulting material was dried and resieved, retaining the 90–125 μm fraction, and this was mounted on to 10 mm diameter aluminium discs using a viscous silicone-based oil. For most of these samples, however, the coarse-grained quartz fraction either did not yield sufficient material for measurement, or large signals from unremovable feldspar inclusions were present and hence a D_E (equivalent dose) value was not estimated.

Standard preparation procedures for fine polymineral grains (4–11 μm) were used (Zimmerman, 1967) and several samples were also subsequently treated with concentrated fluorosilicic acid for 3–7 days in order to yield fine-grained quartz (Rees-Jones, 1995). Polymineralic and quartz fine grains were settled on to aluminium discs from acetone.

Measurement procedures

All luminescence measurements were made using an automated Risø reader, TL-DA-12, fitted with infra-red emitting diodes providing stimulation at 880 ± 80 nm and a filtered halogen lamp as a green light source, which provides wavelengths between 420 and 560 nm (2.9–2.2 eV). Emissions were filtered with two U340 and one BG39 glass filters. An initial 'LISA' (luminescence initial sample assessment) test (Richards and Rhodes, in preparation) was first applied to six discs of each sample in order to determine IRSL and OSL sensitivity. This was used to estimate the D_E value from two single aliquot determinations and to assess the purity of quartz in the case of non-polymineralic samples.

All D_E values were determined using a naturally normalised total integral, multiple aliquot additive dose technique, fitting a single saturating exponential function. Forty-eight aliquots were measured at eight dose points, with the maximum additional beta dose being four to five times the preliminary D_E value. Subtraction of the background luminescence signal was by the last integral subtraction method (Aitken and Xie, 1992). The pre-heat treatment used

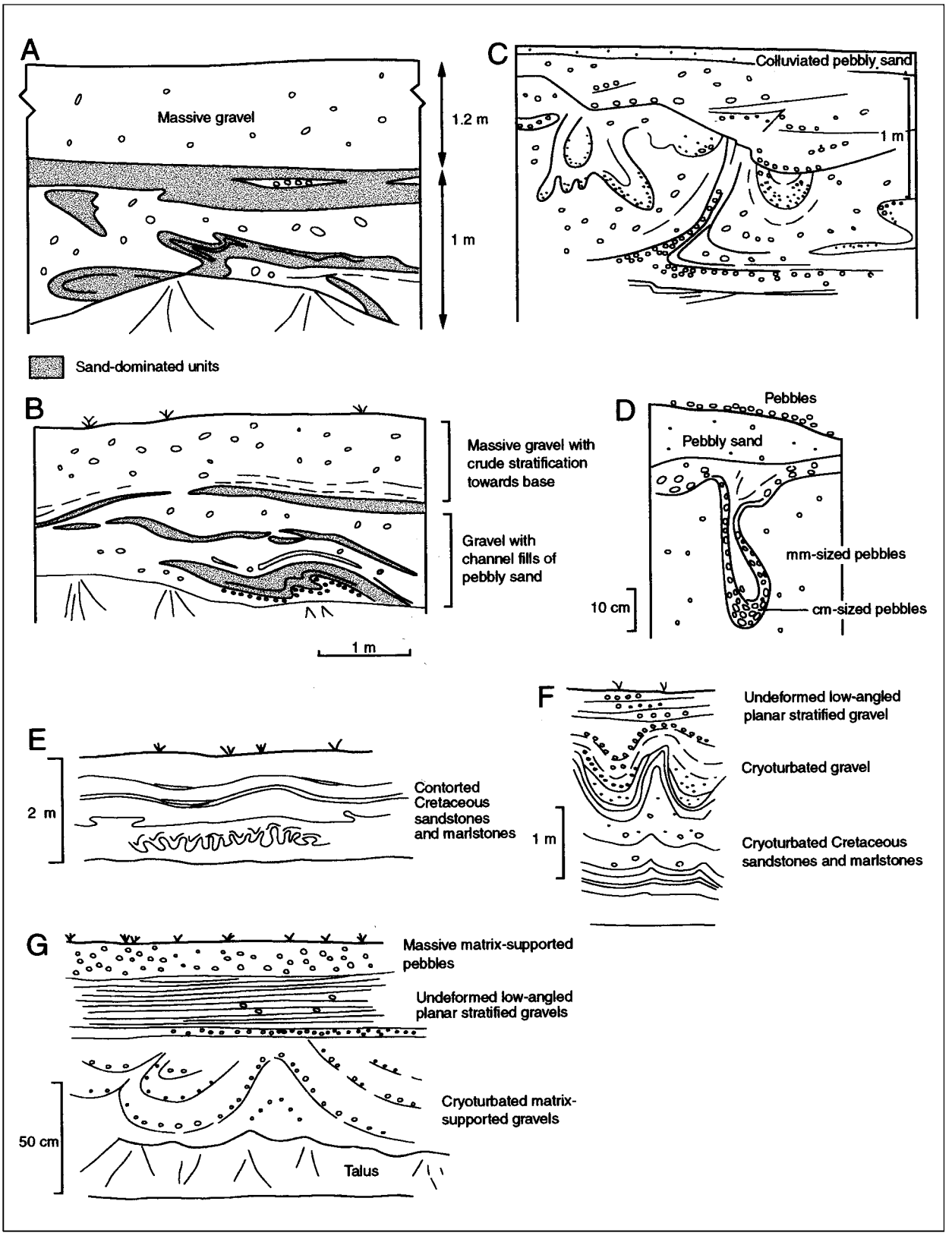

Figure 2 Cryoturbation structures in fanglomerates: (A and B) 44°38.217′N 102°07.192′E; (C and D) 44°26.251′N 102°18.732′E; (E) 44°14.972′N 102°34.158′E; (F) 44°15.013′N 102°33.741′E; (G) 44°22.016′N 102°25.661′E, 1700 m a.s.l. See Fig. 1 for locations.

for all quartz subsamples was 220°C for 5 min and for polymineral samples was 5 days at 100°C followed by 4 h at 160°C. Measurement of all subsamples was carried out (both IRSL and OSL) for 50 s of stimulation at room temperature. In the case of polymineralic samples, IRSL measurement preceded OSL measurement using the same aliquots.

The magnitude of a thermal transfer component in the quartz OSL signal (Rhodes and Bailey, 1997) was determined using a regenerative *X*-axis intercept. In all cases, the magnitude of the thermal transfer signal was found to be insignificant.

Fading tests for both IRSL and OSL were carried out on

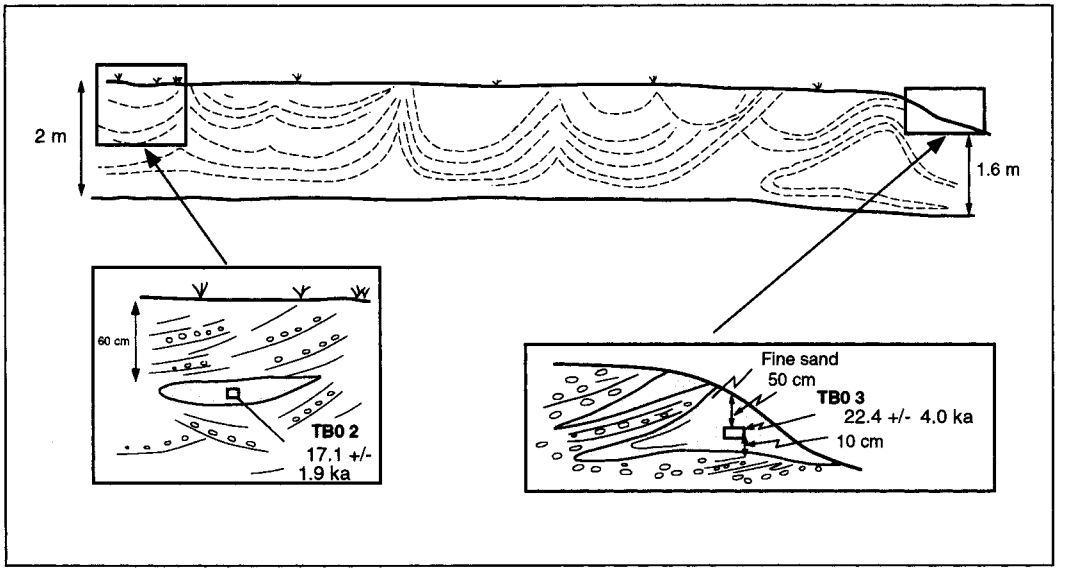

Figure 3 Cryoturbated fanglomerates showing the locations of the sampling sites for luminescence dating at 44°26.396′N 102°15.546′E, 1730 m a.s.l. The fanglomerates comprise decimetre-thick crudely bedded sandy gravel with centimetre-size pebbles and occasional centimetre- to decimetre-thick beds of sand. See Fig. 1 for location.

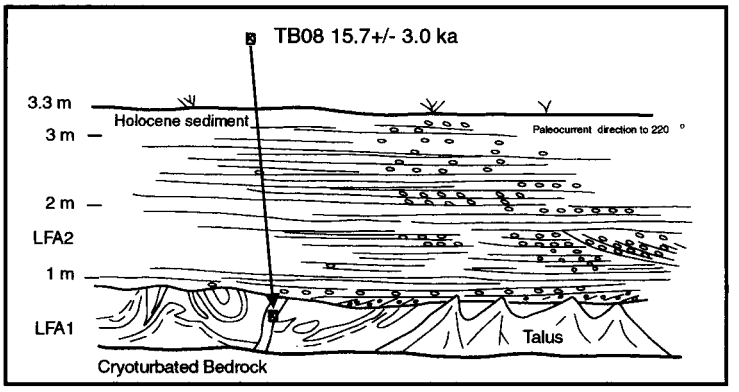

Figure 4 Cryoturbated bedrock comprising Mesozoic marlstones and sandstones overlain by undeformed fanglomerates at 43°41.643′N 102°54.539′E, 1860 m a.s.l., showing the location of the sampling site for luminescence dating within a deformed sand fill. LFA1 comprises cryoturbated purple and blue pebbly marlstone with deformed sand wedges. LFA2 consists of 2–12cm-thick beds of 1–4 cm diameter pebbles that are subangular and are imbricated. Some of these beds have low-angled and trough cross-stratification. See Fig. 1 for location.

most of the subsamples measured, and showed no discernible fading over a 10 day period. Longer term anomalous fading cannot be ruled out for the polymineral subsamples. Where multiple D_E values were measured for the fine-grained samples (both quartz and polymineralic fractions), the measurements were combined to produce a weighted mean D_E value.

The environmental dose rate was calculated from neutron activation analysis of U, Th and K content of each sample. The cosmic dose rate was calculated according to Prescott and Hutton (1994), based on the present depth of overburden and the latitude and altitude of each sample location. The water content measured for each sample was used to calculate environmental radiation attenuation during burial.

Results

Table 1 shows the values used to determine sample ages. Table 2 presents the derived age estimates with depositional environment and location. The D_E values derived from IRSL and OSL of polymineralic samples show no systematic differences and have been combined. Sample TB06 provides the opportunity to compare fine-grained polymineralic, fine-grained quartz and coarse-grained quartz results. This leads to increased confidence in the results, both from the point of view of optical resetting prior to burial and for thermal stability of the luminescence signals.

Samples TB03 and TB05 had coarse-grained quartz results with large uncertainties caused by significant scatter in data. This is attributed to (i) signals from small quantities of feldspar, probably in the form of inclusions, as small IRSL signals were observed that grew with dose, and (ii) incomplete resetting on deposition. A small IRSL signal was also observed for TB06 coarse-grained quartz aliquots, which also grew with dose, but did not appear to lead to significant scatter in the data.

Permafrost structures in the Gobi

Figure 1 shows the location of cryoturbation structures and ice-wedge casts that were recorded during the field work.

Figure 5 Detailed view looking at cryoturbated bedrock comprising Mesozoic marlstones and sandstones that are shown in Fig. 4. Note the sand wedge to the right of the knife and the sand-filled fissure to the right of the plate. See Fig. 1 for location.

Table 1 Values used to calculate luminescence ages. Under column 'Type' FGP refers to fine-grained (4–11 μm) polymineralic (combined IRSL and OSL result), FGQ is fine-grained quartz OSL and CGQ is coarse grained (90–125 μm) quartz. D_E is equivalent dose (in Gy). Uncertainties on INAA analyses of U, Th and K are taken to be 10%. The sample numbers, TB02 to TB08, are the numbers used in the laboratory archive

Sample	Type	U sed. (ppm)	Th sed. (ppm)	K sed.	Cosmic dose rate (μGy/yt^{-1})	Water content	Total dose rate (μGy/yr^{-1})	D_E (Gy)	Age (ka)
TB02	FGP	3.36	8.99	1.89	225	2.0	4990 ± 430	85.1 ± 5.7	17.1 ± 1.9
TB03	FGP	2.27	8.81	2.10	225	2.1	4660 ± 370	104.4 ± 16.5	22.4 ± 4.0
TB04	FGQ	1.61	10.5	1.99	205	17	3220 ± 500	60.6 ± 4.2	18.8 ± 3.2
TB05	FGP	2.85	7.84	2.01	220	13	4120 ± 700	53.3 ± 4.8	12.9 ± 2.5
TB06	FGP	0.70	3.83	2.01	185	0.8	3160 ± 240	33.4 ± 2.3	10.6 ± 1.1
TB06	FGQ	0.70	3.83	2.01	185	0.8	2940 ± 240	28.9 ± 11.3	9.8 ± 3.9
TB06	CGQ	0.70	3.83	2.01	185	0.8	2670 ± 220	37.2 ± 6.9	14.0 ± 2.8
TB07	FGP	0.68	3.43	2.29	210	1.4	3380 ± 270	14.5 ± 1.1	4.3 ± 0.5
TB08	FGP	1.27	4.32	1.87	205	5.1	3200 ± 310	50.4 ± 8.3	15.7 ± 3.0

Table 2 Results for dated luminescence samples. Under column 'Type' FGP refers to fine-grained (4–11 μm) polymineralic (combined IRSL and OSL results), FGQ is fine-grained quartz OSL, FGP-Q is combined FGP and FGQ results and CGQ is coarse-grained (90–125 μm) quartz

Sample	Age (ka)	Lithology	Environment of deposition	Type	Location
TB02	17.1 ± 1.9	Fine sand	Cryoturbated fanglomerate	FGP	44°26.396'N/102°15.546'E
TB03	22.4 ± 4.0	Fine sand	Cryoturbated fanglomerate	FGP	44°26.396'N/102°15.546'E
TB04	18.8 ± 3.2	Sandy silt	Cryoturbated distal fanglomerate	FGQ	44°25.09'N/102°19.78'E
TB05	12.9 ± 22.5	Fine sand	Undeformed distal fanglomerate	FGP	44°25.09'N/102°19.78'E
TB06	10.6 ± 1.1 14.0 ± 2.8	Medium sand	Fluvial sediment	FGP-Q CGQ	43°43.755'N/102°22.315'E
TB07	4.3 ± 0.5	Fine–medium sand	Fluvial sediment	FGP	44°22.016'N/102°15.661'E
TB08	15.7 ± 3.0	Medium sand	Ice-wedge cast fill	FGP	43°41.643'N/102°15.546'E

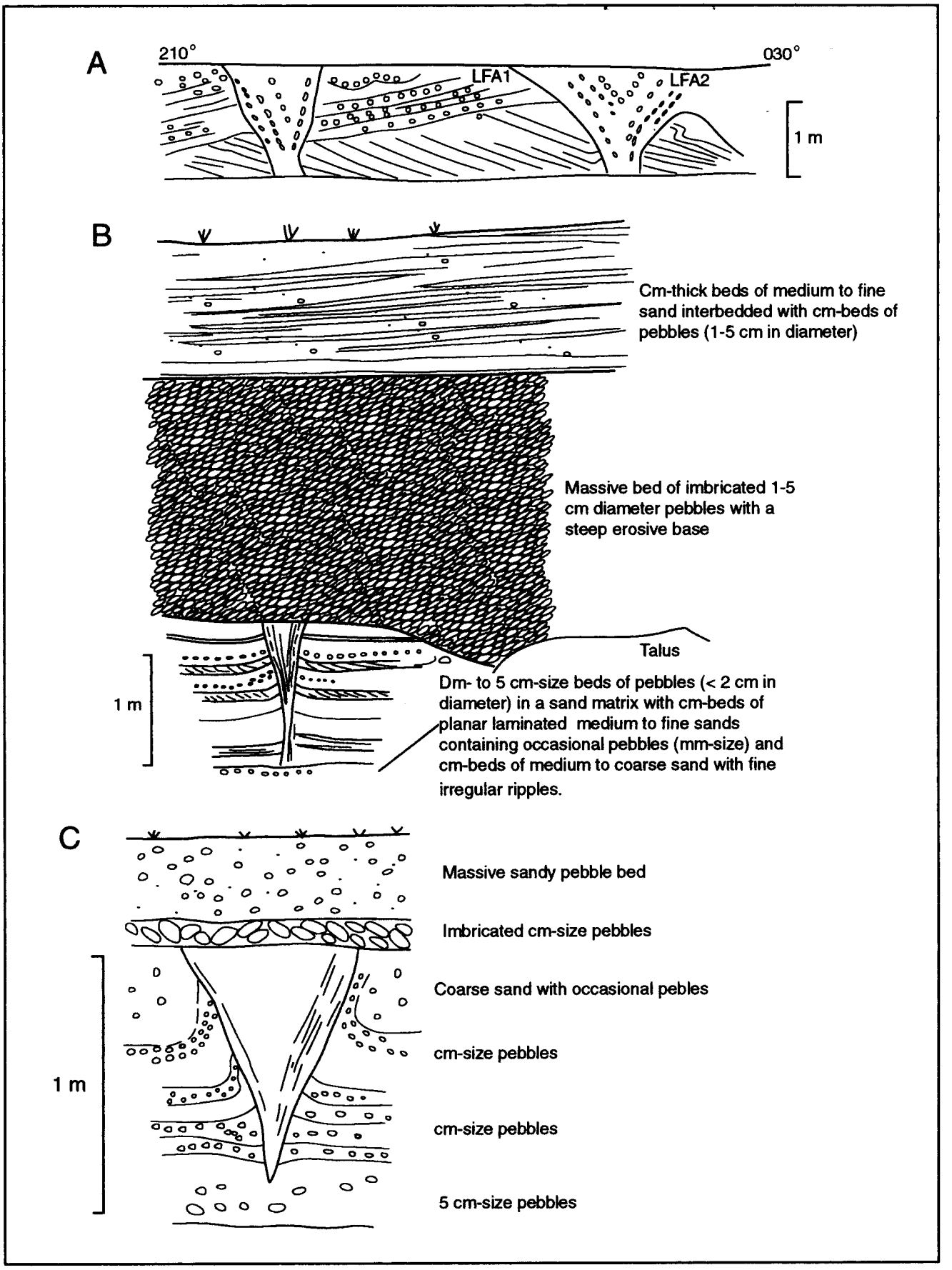

Figure 6 Ice-wedge casts: (A) 43°42.295'N 102°54.982'E, 1950 m a.s.l.; (B) 43°43.199'N 102°22.509'E; (C) 44°22.016'N 102°25.661'E, 1700 m a.s.l. See Fig. 1 for locations.

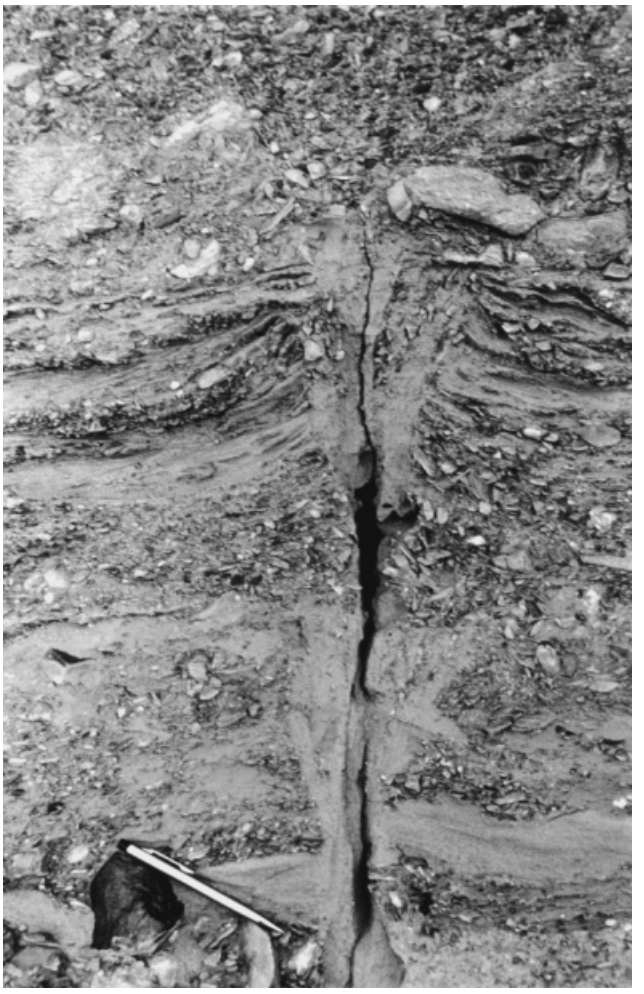

Figure 7 Ice-wedge cast at 43°43.199′N 102°22.502′E. See Fig. 1 for location.

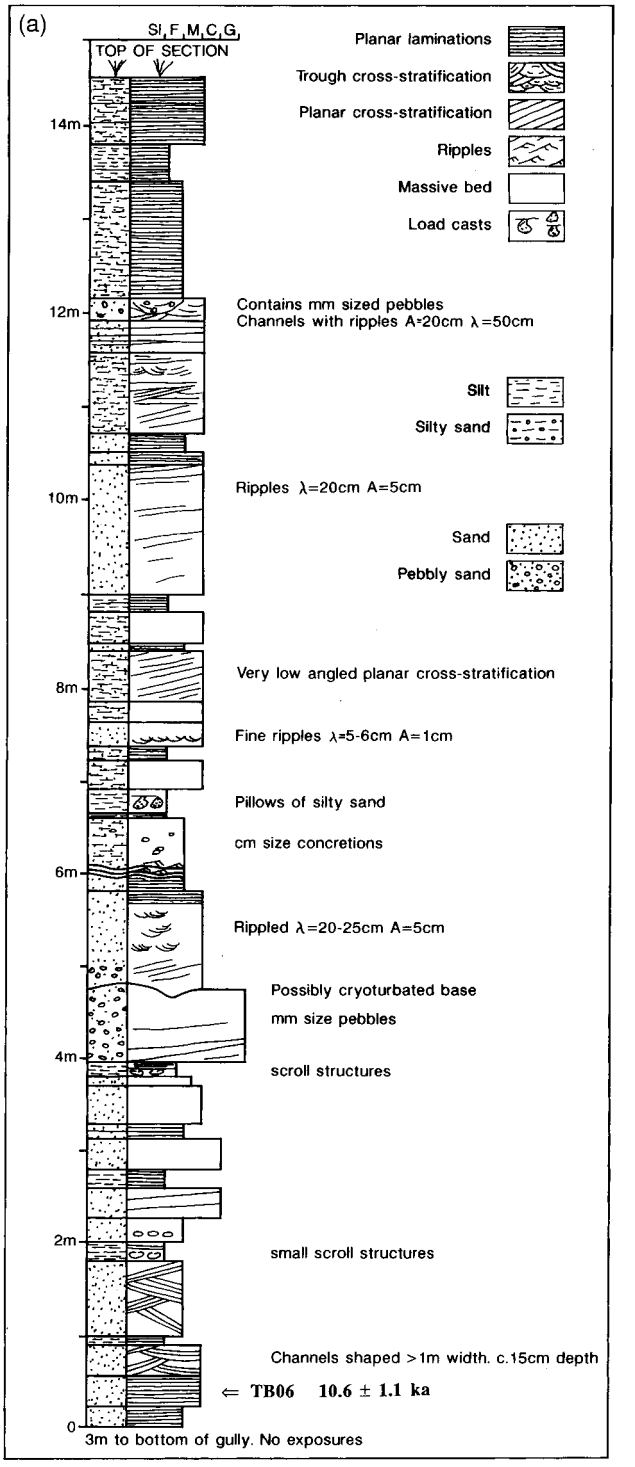

Figure 8 Sections through uncryoturbated fluvial deposits at (a) 43°43.755′N 102°22.315′E and (b) 43°37.420′N 102°50.229′E. See Fig. 1 for location.

Both sets of structures occur in unconsolidated Quaternary fanglomerates and Mesozoic bedrock (Figs 2 to 9). In this region, the cryoturbation structures are essentially involuted sediment and rock. Although involutions may be produced by other mechanisms, such as sediment loading or liquefaction during earthquakes, the occurrence of ice-wedge casts in the same stratigraphic horizons supports the view that the involutions studied in this region are the result of active layer and permafrost processes. These involutions, therefore, can be called cryoturbation structures.

The cryoturbation structures have a large range of forms and include: individual folds with small amplitudes (10–20 cm) and large wavelengths (approximately 2 m) (Fig. 2E; type 1 of Vandenberghe, 1988); highly irregular decimeter-size involutions (Fig. 2A, B and C: type 6 of Vandenberghe, 1988); solitary 'teardrop' of diapiric forms (Fig. 2D: type 4 of Vandenberghe, 1988); and fairly regular symmetrical convolutions with large amplitudes of 0.5 to 2 m (Figs 3 and 4: type 2b of Vandenberghe, 1988) and small amplitudes of decimetre size (Figs 2E, F and G; type 3 of Vandenberghe, 1988). At many locations the horizons containing cryoturbation structures and the cryoturbation structures themselves are truncated (Fig. 3) and are overlain by undeformed low-angled planar stratified fanglomerates (Figs 2C, F and G). The cryoturbation layers have a maximum thickness of approximately 2 m below the undeformed fanglomerates, or where the sections are deformed throughout they occur to a maximum depth of 2 m below the present surface. Sand samples (TB02 and TB03) taken from within cryoturbated horizons are dated at 22.4 ± 4.0 ka and 17.1 ± 1.9 ka (Fig. 3 and Table 2).

The ice-wedge casts that are present in the Gobi exhibit the main diagnostic characteristics described by Johnsson (1959), Black (1976) and Ballantyne and Harris (1994), namely they taper downwards to a point, the host sediment is upturned against the side of the cast, the infilling sediment has slump structures, and pebbles within the fills are verti-

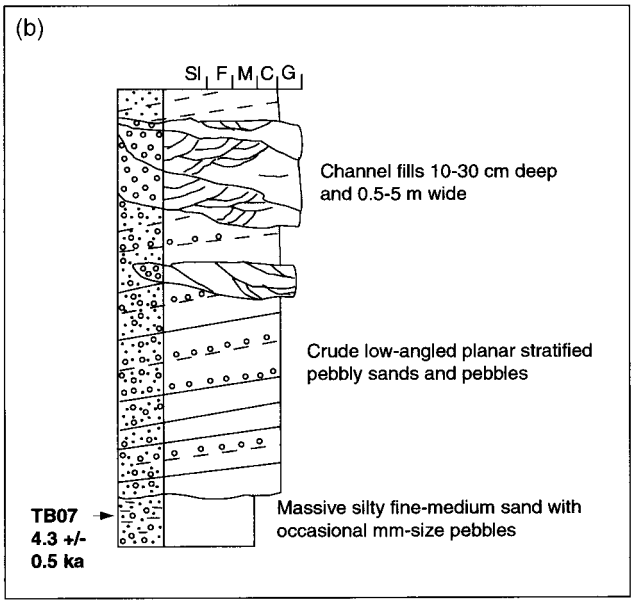

Figure 8 Continued.

cally aligned (Figs 6 and 7). Sand wedges are also present at some locations and extend to depths of as much as 1 m below the palaeosurface. Figures 4 and 5 show a sand wedge and a deformed sand fill that cross-cut the cryoturbation structures. A sample of sand was collected from the sand fill and was dated to 15.7 ± 3.0 ka (Fig. 4; Table 2).

Luminescence dates for sediments stratigraphically above the cryoturbated units yield ages of 4.3 ± 0.5 ka, 10.6 ± 1.1 ka and 12.9 ± 2.5 ka (Figs 8 and 9). In the latter case (Fig. 9), the underlying cryoturbated sediments have an age of 18.8 ± 3.2 ka.

Discussion

The luminescence dates within the cryoturbated fanglomerates (TB02 = 17.1 ± 1.9 ka, TB03 = 22.4 ± 4.0 ka and TB04 = 18.8 ± 3.2 ka) and on the deformed sand fill within cryoturbated bedrock (TB08 = 15.7 ± 3.0 ka) show that these sediments were deposited during the latter part of the Last Glacial. These sediments were subsequently cryoturbated by active layer processes that must have occurred during late Pleistocene times, that is, contemporaneously and/or after about 22 to 15 ka. The cryoturbation structures, however, must have formed before the deposition of the undeformed sediments that overlie the cryoturbated sediments that are younger than about 13–10 ka (TB05 = 12.9 ± 2.5 ka, TB06 = 10.6 ± 1.1 ka and TB07 = 4.3 ± 0.5 ka). These data, therefore, support the view that active layer processes and permafrost was developed in the desert floors and alluvial fans in this region during Last Glacial times, but that the permafrost degraded towards the end of the Pleistocene (after about 13–10 ka) and was absent during Holocene times.

The occurrence of ice-cast wedges in sand and gravel indicates severe winter ground cooling with continuous permafrost and mean annual air temperatures below approximately –6°C (Péwé, 1966; Washburn, 1979, 1980; Harry and Gozdzik, 1988; Burn, 1990; Ballantyne and Harris, 1994). The nature of the cryoturbation structures suggest that there must have been adequate water available for their formation and the structures may indicate that the maximum depth of annual freeze–thaw in this region was probably about 2 m. This is a maximum depth of annual freeze–thaw because syndepositional sedimentation may have increased the thickness of the deformation under periglacial conditions, with lower structures being older than upper structures. The absence of active layer or permafrost structures in the southern- and westernmost areas probably relates to an insufficient supply of ground water and/or to the fact that the mean annual air temperatures were close to 0°C. These permafrost

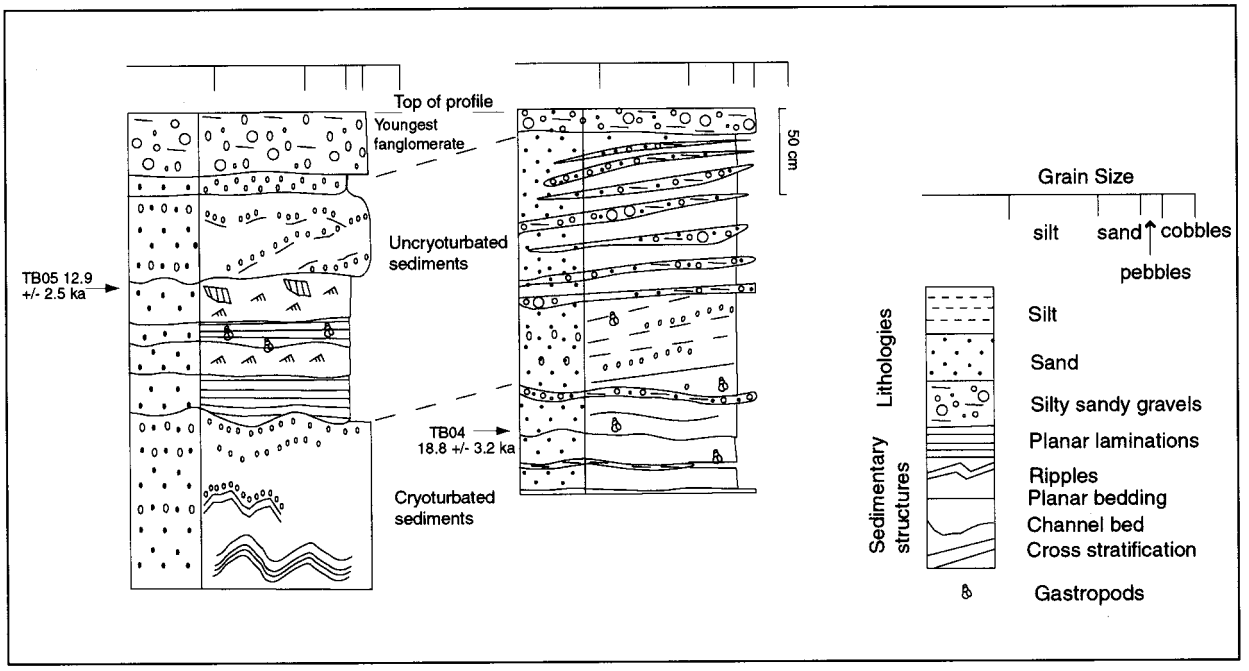

Figure 9 Sections in distal alluvial fan sediments at 44°25.09′N 102°19.783′E. The two sections are about 100 m apart and sample TB05 was taken from uncryoturbated sediment, whereas sample TB04 was from cryoturbated sediment. See Fig. 1 for location.

structures are, therefore, significant for marking the southernmost evidence of northern Asia permafrost during the latter part of the Last Glacial.

Conclusions

Luminescence dates constrain the age of permafrost development to the latter part of the Last Glacial and indicate that permafrost degradation occurred during Lateglacial times and that permafrost in the desert floors and alluvial fans in the Gobi was absent during the Holocene. The active layer and permafrost structures mark the southern evidence of north Asian permafrost during the Last Glacial and suggest that mean annual air temperatures were below approximately –6°C.

Acknowledgements This research was undertaken as part of NERC grant GR9/01881 awarded to BFW and LAO and NERC studentship GT4/95/199/E awarded to BR. We would like to acknowledge Colin Ballantyne and an anonymous referee for their careful review and comments on this paper. Thanks also goes to Christoph Lehmann for drafting the figures.

References

AITKEN, M. J. and XIE, J. 1992. Optical dating using infrared diodes: young samples. *Quaternary Science Reviews*, **11**, 147–152.

BALLANTYNE, C. K. and HARRIS, C. 1994. *The Periglaciation of Great Britain*. Cambridge University Press, Cambridge.

BLACK, R. F. 1976. Periglacial features indicative of permafrost: ice and soil wedges. *Quaternary Research*, **6**, 3–26.

BURN, C. R. 1990. Implications for palaeoenvironmental reconstruction of recent ice-wedge development at Mayo, Yukon Territory. *Permafrost and Periglacial Processes*, **1**, 3–14.

DEVYATKIN, E. V. 1981. *The Cenozoic of Inner Asia*. Joint Soviet–Mongolian Scientific Research Geological Expedition, Transactions Vol. 27, Nauka, Moscow.

GRAVIS, G. F. (ed.) 1974. *Geocryological Conditions of Mongolian Peoples Republic*. Moscow. (In Russian).

HARRY, D. G. and GOZDZIK, J. S. 1988. Ice wedges: growth, thaw transformation, and palaeoenvironmental significance. *Journal of Quaternary Science*, **3**, 39–55.

JOHNSSON, G. 1959. True and false ice-wedges in southern Sweden. *Geografiska Annaler*, **41**, 15–33.

OWEN, L. A., WINDLEY, B. F., CUNNINGHAM, W. D., BADAMGAROV, G. and DORJNAMJAA, D. 1996. Quaternary alluvial fans in the Gobi Desert, southern Mongolia: evidence for neotectonics and climate change. *Journal of Quaternary Science*, **12**, 3, 239–252.

PEWE, T. L. 1966. Palaeoclimatic significance of fossil ice wedges. *Biuletyn Peryglacjalny*, **15**, 65–73.

PRESCOTT, J. R. and HUTTON, J. T. 1994. Cosmic ray contributions to dose rates for luminescence and ESR dating: large depths and long-term time variations. *Radiation Measurements*, **23**, 497–500.

REES-JONES, J. 1995. Optical dating of young sediments using fine-grain quartz. *Ancient TL*, **13**(2), 9–14.

RHODES, E. J. and BAILEY, R. M. 1997. Thermal transfer effects observed in the luminescence of quartz from recent glacio-fluvial sediments. *Quaternary Geochronology (Quaternary Science Reviews)*, **16**, 291–298.

VANDENBERGHE, J. 1988. Cryoturbations. IN: CLARKE, M. J. (ed.), *Advances in Periglacial Geomorphology*, 179–198. Wiley, Chichester.

WASHBURN, A. L. 1979. *Geocryology: a Survey of Periglacial Processes and Environments*. Edward Arnold, London.

WASHBURN, A. L. 1980. Permafrost features as evidence of climate change. *Earth Science Reviews*, **15**, 327–402.

ZIMMERMAN, D. W. 1967. Thermoluminescence from fine grains from ancient pottery. *Archaeometry*, **10**, 26–28.